High optical to X-ray polarization ratio reveals Compton scattering in BL Lacertae's jet

Iván Agudo [iD],[1] Ioannis Liodakis [iD],[2,3] Jorge Otero-Santos [iD],[1,4] Riccardo Middei [iD],[5,6,7] Alan Marscher [iD],[8]
Svetlana Jorstad [iD],[8,9] Haocheng Zhang [iD],[10,11] Hui Li [iD],[12] Laura Di Gesu [iD],[13] Roger W. Romani [iD],[14]
Dawoon E. Kim [iD],[15,16,17] Francesco Fenu [iD],[13] Herman L. Marshall [iD],[18] Luigi Pacciani [iD],[15]
Juan Escudero Pedrosa [iD],[1,7] Francisco José Aceituno [iD],[1] Beatriz Agís-González [iD],[3,1] Giacomo Bonnoli [iD],[19,1]
Víctor Casanova [iD],[1] Daniel Morcuende [iD],[1] Vilppu Piirola [iD],[20] Alfredo Sota [iD],[1] Pouya M. Kouch [iD],[20,21]
Elina Lindfors [iD],[20] Callum McCall [iD],[22] Helen E. Jermak [iD],[22] Iain A. Steele,[22] George A. Borman [iD],[23]
Tatiana S. Grishina [iD],[9] Vladimir A. Hagen-Thorn [iD],[9] Evgenia N. Kopatskaya [iD],[9] Elena G. Larionova [iD],[9]
Daria A. Morozova [iD],[9] Sergey S. Savchenko [iD],[9,24] Ekaterina V. Shishkina [iD],[9] Ivan S. Troitskiy [iD],[9]
Yulia V. Troitskaya [iD],[9] Andrey A. Vasilyev [iD],[9] Alexey V. Zhovtan,[23] Ioannis Myserlis [iD],[25,26]
Mark Gurwell [iD],[7] Garrett Keating [iD],[7] Ramprasad Rao [iD],[7] Sincheol Kang [iD],[27] Sang-Sung Lee [iD],[27,28]
Sanghyun Kim [iD],[27,28] Whee Yeon Cheong [iD],[27,28] Hyeon-Woo Jeong [iD],[27,28] Emmanouil Angelakis [iD],[29]
Alexander Kraus [iD],[26] Dmitry Blinov [iD],[3,30] Siddharth Maharana [iD],[31] Rumen Bachev,[32]
Jenni Jormanainen [iD],[20,21] Kari Nilsson [iD],[21] Vandad Fallah Ramazani [iD],[21,33] Carolina Casadio [iD],[3,30]
Antonio Fuentes [iD],[1] Efthalia Traianou [iD],[1] Clemens Thum [iD],[25] José L. Gómez,[1] Lucio Angelo Antonelli [iD],[6]
Matteo Bachetti [iD],[34] Luca Baldini [iD],[35,36] Wayne H. Baumgartner [iD],[2] Ronaldo Bellazzini [iD],[35]
Stefano Bianchi [iD],[37] Stephen D. Bongiorno [iD],[2] Raffaella Bonino [iD],[38,39] Alessandro Brez [iD],[35]
Niccolò Bucciantini [iD],[40,41,42] Fiamma Capitanio [iD],[15] Simone Castellano [iD],[35] Elisabetta Cavazzuti [iD],[13]
Chien-Ting Chen [iD],[43] Stefano Ciprini [iD],[44,5] Enrico Costa [iD],[15] Alessandra De Rosa [iD],[15]
Ettore Del Monte [iD],[15] Niccolò Di Lalla [iD],[14] Alessandro Di Marco [iD],[15] Immacolata Donnarumma [iD],[13]
Victor Doroshenko [iD],[45] Michal Dovčiak [iD],[46] Steven R. Ehlert [iD],[2] Teruaki Enoto [iD],[47] Yuri Evangelista [iD],[15]
Sergio Fabiani [iD],[15] Riccardo Ferrazzoli [iD],[15] Javier A. García [iD],[11] Shuichi Gunji [iD],[48] Kiyoshi Hayashida,[49]
Jeremy Heyl [iD],[50] Wataru Iwakiri [iD],[51] Philip Kaaret [iD],[2] Vladimir Karas [iD],[46] Fabian Kislat [iD],[52]
Takao Kitaguchi,[47] Jeffery J. Kolodziejczak [iD],[2] Henric Krawczynski [iD],[53] Fabio La Monaca [iD],[15,17]
Luca Latronico [iD],[38] Simone Maldera [iD],[38] Alberto Manfreda [iD],[54] Frédéric Marin [iD],[55] Andrea Marinucci [iD],[13]
Francesco Massaro [iD],[38,39] Giorgio Matt [iD],[37] Ikuyuki Mitsuishi,[56] Tsunefumi Mizuno [iD],[57] Fabio Muleri [iD],[15]
Michela Negro [iD],[58] Chi-Yung Ng [iD],[59] Stephen L. O'Dell [iD],[2] Nicola Omodei [iD],[14] Chiara Oppedisano [iD],[38]
Alessandro Papitto [iD],[6] George G. Pavlov [iD],[60] Abel L. Peirson [iD],[14] Matteo Perri [iD],[5,6]
Melissa Pesce-Rollins [iD],[35] Pierre-Olivier Petrucci [iD],[61] Maura Pilia [iD],[34] Andrea Possenti [iD],[34]
Juri Poutanen [iD],[20] Simonetta Puccetti [iD],[5] Brian D. Ramsey [iD],[2] John Rankin [iD],[15] Ajay Ratheesh [iD],[15]
Oliver J. Roberts [iD],[43] Carmelo Sgrò [iD],[35] Patrick Slane [iD],[7] Paolo Soffitta [iD],[15] Gloria Spandre [iD],[35]
Douglas A. Swartz [iD],[43] Toru Tamagawa [iD],[47] Fabrizio Tavecchio [iD],[19] Roberto Taverna [iD],[62] Yuzuru Tawara,[56]
Allyn F. Tennant [iD],[2] Nicholas E. Thomas [iD],[2] Francesco Tombesi [iD],[17,44] Alessio Trois [iD],[34]
Sergey S. Tsygankov [iD],[20] Roberto Turolla [iD],[62,63] Jacco Vink [iD],[64] Martin C. Weisskopf [iD],[2] Kinwah Wu [iD],[63]
Fei Xie [iD],[65,15] and Silvia Zane [iD][63]

[1] Instituto de Astrofísica de Andalucía, IAA-CSIC, Glorieta de la Astronomía s/n, E-18008 Granada, Spain
[2] NASA Marshall Space Flight Center, Huntsville, AL 35812, USA
[3] Institute of Astrophysics, Foundation for Research and Technology - Hellas, Voutes, 7110, Heraklion, Greece
[4] Istituto Nazionale di Fisica Nucleare, Sezione di Padova, 35131 Padova, Italy
[5] Space Science Data Center, Agenzia Spaziale Italiana, Via del Politecnico snc, I-00133 Roma, Italy
[6] INAF Osservatorio Astronomico di Roma, Via Frascati 33, 00078 Monte Porzio Catone (RM), Italy
[7] Center for Astrophysics | Harvard & Smithsonian, 60 Garden Street, Cambridge, MA 02138 USA
[8] Institute for Astrophysical Research, Boston University, 725 Commonwealth Avenue, Boston, MA 02215, USA
[9] Saint Petersburg State University, 7/9 Universitetskaya nab., St. Petersburg, 199034 Russia
[10] University of Maryland Baltimore County, Baltimore, MD 21250, USA
[11] NASA Goddard Space Flight Center, Greenbelt, MD 20771, USA
[12] Theoretical Division, Los Alamos National Laboratory, Los Alamos, NM 87545, USA

Corresponding author: Iván Agudo, Ioannis Liodakis, Jorge Otero-Santos, Riccardo Middei, Alan Marscher
iagudo@iaa.es, yannis.liodakis@gmail.com, jorge.otero@pd.infn.it, riccardo.middei@ssdc.asi.it, marscher@bu.edu

arXiv:2505.01832v1 [astro-ph.HE] 3 May 2025

2

[13] ASI - Agenzia Spaziale Italiana, Via del Politecnico snc, 00133 Roma, Italy

[14] Department of Physics and Kavli Institute for Particle Astrophysics and Cosmology, Stanford University, Stanford, California 94305, USA

[15] INAF, Istituto di Astrofisica e Planetologia Spaziali, Via Fosso del Cavaliere 100, 00133 Roma, Italy

[16] Dipartimento di Fisica, Universitá degli Studi di Roma "La Sapienza", Piazzale Aldo Moro 5, 00185 Roma, Italy

[17] Dipartimento di Fisica, Universitá degli Studi di Roma "Tor Vergata", Via della Ricerca Scientifica 1, 00133 Roma, Italy

[18] MIT Kavli Institute for Astrophysics and Space Research, Massachusetts Institute of Technology, 77 Massachusetts Avenue, Cambridge, MA 02139, USA

[19] INAF Osservatorio Astronomico di Brera, Via E. Bianchi 46, 23807 Merate (LC), Italy

[20] Department of Physics and Astronomy, Quantum, Vesilinnantie 5, FI-20014 University of Turku, Finland

[21] Finnish Centre for Astronomy with ESO (FINCA), 20014 University of Turku, Finland

[22] Astrophysics Research Institute, Liverpool John Moores University, Liverpool Science Park IC2, 146 Brownlow Hill, UK

[23] Crimean Astrophysical Observatory RAS, P/O Nauchny, 298409, Crimea

[24] Pulkovo Observatory, St.Petersburg, 196140, Russia

[25] Institut de Radioastronomie Millimétrique, Avenida Divina Pastora, 7, Local 20, E-18012 Granada, Spain

[26] Max-Planck-Institut für Radioastronomie, Auf dem Hügel 69, D-53121 Bonn, Germany

[27] Korea Astronomy and Space Science Institute, 776 Daedeok-daero, Yuseong-gu, Daejeon 34055, Korea

[28] University of Science and Technology, Korea, 217 Gajeong-ro, Yuseong-gu, Daejeon 34113, Korea

[29] Orchideenweg 8, 53123 Bonn, Germany

[30] Department of Physics, University of Crete, 70013, Heraklion, Greece

[31] South African Astronomical Observatory, PO Box 9, Observatory, 7935, Cape Town, South Africa

[32] Institute of Astronomy and NAO, Bulgarian Academy of Sciences, 1784 Sofia, Bulgaria

[33] Aalto University Metsähovi Radio Observatory, Metsähovintie 114, FI-02540 Kylmälä, Finland

[34] INAF Osservatorio Astronomico di Cagliari, Via della Scienza 5, 09047 Selargius (CA), Italy

[35] Istituto Nazionale di Fisica Nucleare, Sezione di Pisa, Largo B. Pontecorvo 3, 56127 Pisa, Italy

[36] Dipartimento di Fisica, Universitá di Pisa, Largo B. Pontecorvo 3, 56127 Pisa, Italy

[37] Dipartimento di Matematica e Fisica, Universitá degli Studi Roma Tre, Via della Vasca Navale 84, 00146 Roma, Italy

[38] Istituto Nazionale di Fisica Nucleare, Sezione di Torino, Via Pietro Giuria 1, 10125 Torino, Italy

[39] Dipartimento di Fisica, Universitá degli Studi di Torino, Via Pietro Giuria 1, 10125 Torino, Italy

[40] INAF Osservatorio Astrofisico di Arcetri, Largo Enrico Fermi 5, 50125 Firenze, Italy

[41] Dipartimento di Fisica e Astronomia, Universitá degli Studi di Firenze, Via Sansone 1, 50019 Sesto Fiorentino (FI), Italy

[42] Istituto Nazionale di Fisica Nucleare, Sezione di Firenze, Via Sansone 1, 50019 Sesto Fiorentino (FI), Italy

[43] Science and Technology Institute, Universities Space Research Association, Huntsville, AL 35805, USA

[44] Istituto Nazionale di Fisica Nucleare, Sezione di Roma "Tor Vergata", Via della Ricerca Scientifica 1, 00133 Roma, Italy

[45] Institut für Astronomie und Astrophysik, Universität Tübingen, Sand 1, 72076 Tübingen, Germany

[46] Astronomical Institute of the Czech Academy of Sciences, Bočn(i) II 1401/1, 14100 Praha 4, Czech Republic

[47] RIKEN Cluster for Pioneering Research, 2-1 Hirosawa, Wako, Saitama 351-0198, Japan

[48] Yamagata University,1-4-12 Kojirakawa-machi, Yamagata-shi 990-8560, Japan

[49] Osaka University, 1-1 Yamadaoka, Suita, Osaka 565-0871, Japan

[50] University of British Columbia, Vancouver, BC V6T 1Z4, Canada

[51] International Center for Hadron Astrophysics, Chiba University, Chiba 263-8522, Japan

[52] Department of Physics and Astronomy and Space Science Center, University of New Hampshire, Durham, NH 03824, USA

[53] Physics Department and McDonnell Center for the Space Sciences, Washington University in St. Louis, St. Louis, MO 63130, USA

[54] Istituto Nazionale di Fisica Nucleare, Sezione di Napoli, Strada Comunale Cinthia, 80126 Napoli, Italy

[55] Université de Strasbourg, CNRS, Observatoire Astronomique de Strasbourg, UMR 7550, 67000 Strasbourg, France

[56] Graduate School of Science, Division of Particle and Astrophysical Science, Nagoya University, Furo-cho, Chikusa-ku, Nagoya, Aichi 464-8602, Japan

[57] Hiroshima Astrophysical Science Center, Hiroshima University, 1-3-1 Kagamiyama, Higashi-Hiroshima, Hiroshima 739-8526, Japan

[58] Department of Physics and Astronomy, Louisiana State University, Baton Rouge, LA 70803, USA

[59] Department of Physics, The University of Hong Kong, Pokfulam, Hong Kong

[60] Department of Astronomy and Astrophysics, Pennsylvania State University, University Park, PA 16802, USA

[61] Université Grenoble Alpes, CNRS, IPAG, 38000 Grenoble, France

[62] Dipartimento di Fisica e Astronomia, Universitá degli Studi di Padova, Via Marzolo 8, 35131 Padova, Italy

[63] Mullard Space Science Laboratory, University College London, Holmbury St Mary, Dorking, Surrey RH5 6NT, UK

[64] Anton Pannekoek Institute for Astronomy & GRAPPA, University of Amsterdam, Science Park 904, 1098 XH Amsterdam, The Netherlands

[65] *Guangxi Key Laboratory for Relativistic Astrophysics, School of Physical Science and Technology, Guangxi University, Nanning 530004, China*

ABSTRACT

Blazars, supermassive black hole systems (SMBHs) with highly relativistic jets aligned with the line of sight, are the most powerful long-lived emitters of electromagnetic emission in the Universe. We report here on a radio to gamma-ray multiwavelength campaign on the blazar BL Lacertae with unprecedented polarimetric coverage from radio to X-ray wavelengths. The observations caught an extraordinary event on 2023 November 10-18, when the degree of linear polarization of optical synchrotron radiation reached a record value of 47.5%. In stark contrast, the Imaging X-ray Polarimetry Explorer (IXPE) found that the X-ray (Compton scattering or hadron-induced) emission was polarized at less than 7.4% (3σ confidence level). We argue here that this observational result rules out a hadronic origin of the high energy emission, and strongly favors a leptonic (Compton scattering) origin, thereby breaking the degeneracy between hadronic and leptonic emission models for BL Lacertae and demonstrating the power of multiwavelength polarimetry to address this question. Furthermore, the multiwavelength flux and polarization variability, featuring an extremely prominent rise and decay of the optical polarization degree, is interpreted for the first time by the relaxation of a magnetic "spring" embedded in the newly injected plasma. This suggests that the plasma jet can maintain a predominant toroidal magnetic field component parsecs away from the central engine.

1. INTRODUCTION

The most remarkable properties of blazars, the most powerful class of active galactic nuclei, whose relativistic jets point at a small angle to the line of sight (Blandford et al. 2019), are produced by light-travel effects and relativistic aberration of their broadband radiation. While it is well established that the low-energy component of the spectral energy distribution (SED) of blazars is dominated by non-thermal synchrotron radiation, the nature of their high-energy emission component is a pressing question in high-energy astrophysics. Models based on both leptonic (Maraschi et al. 1992; Dermer & Schlickeiser 1993) and hadronic (Aharonian 2000) origins of this radiation have been proposed, however without solid evidence to rule out one or the other (see Hovatta & Lindfors 2019, and references therein). The latter requires the presence of highly relativistic protons accelerated in the jet. If hadronic processes were confirmed, SMBH jets would be the most plausible candidates for the origin of the recently observed extragalactic high-energy neutrinos (IceCube Collaboration et al. 2018) and ultra high-energy cosmic rays (e.g., Telescope Array Collaboration et al. 2023). This would offer new ways for studying fundamental particle physics in extreme regimes. Simultaneous broadband polarimetry from radio wavelengths to X-rays, which is now possible thanks to the novel capabilities of the Imaging X-ray Polarimetry Explorer (IXPE, Weisskopf et al. 2022), can finally settle this debate, as different models predict different behaviors of the low- and high-energy polarized emission (e.g., Zhang & Böttcher 2013; Peirson & Romani 2019; Peirson et al. 2022).

Blazars are prime candidates for such studies. In particular, those blazars where the emission of the low-energy component peaks at infrared frequencies, namely low- (LSP) and intermediate-synchrotron-peaked (ISP) blazars (Abdo et al. 2010), are ideal targets for investigating the origin of the high-energy emission, as their X-ray emission arises mainly from the high-energy component. BL Lacertae (BL Lac), the archetype of the BL Lac subclass of blazars, is often classified as LSP, with $\nu_{\rm syn} \approx 4 \times 10^{13}$ Hz (see Ajello et al. 2020; Lott et al. 2020). However, during some flaring states it becomes an ISP blazar ($\nu_{\rm syn} > 10^{14}$ Hz). BL Lac has been the target of three previous IXPE observations (Middei et al. 2023; Peirson et al. 2023), two in the LSP and one in the ISP state. Thus far, polarization in the IXPE 2-8 keV band remains undetected, although during the ISP state observed in November 2022, Peirson et al. (2023) reported significant polarization of $\sim$22% in the 2-4 keV sub-band.
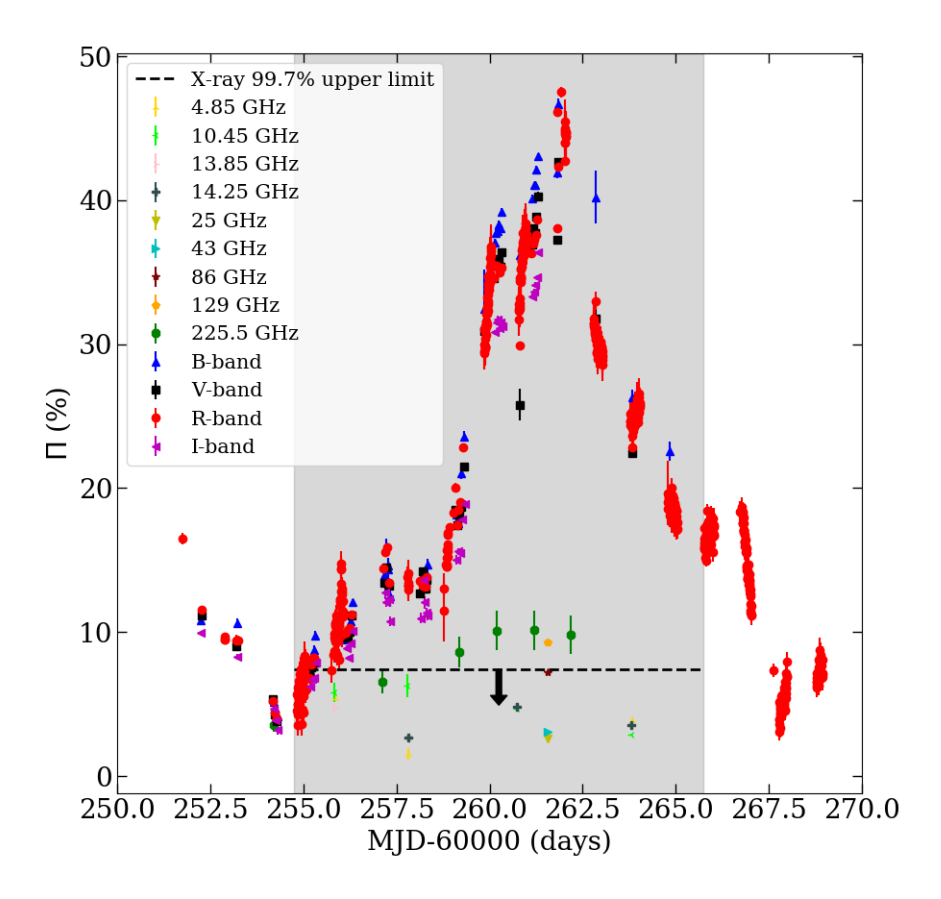
Figure 1. Multiwavelength polarization measurements during the IXPE observing campaign reported here. The grey shaded area marks the duration of the IXPE observation. The different radio and millimeter observing wavelengths and optical bands are marked with different symbols and colors, as shown in the legend. The 99.73% (3σ) upper limit of the entire integrated IXPE observation is marked with the black horizontal dashed line and arrow. The error bars correspond to the 68% (1σ) confidence interval of every measurement. MJD 60250 corresponds to November 2, 2023.

2. RESULTS

BL Lac was observed by IXPE for approximately 500 ks during 2023 November 7-17. These observations were made during a low state of emission in the γ-ray range, although the flux in the synchrotron dominated spectral ranges was elevated. In particular, at short mm wavelengths the flux was at the highest level ever reported, while the optical and X-ray fluxes were at moderately high levels; see Figure 2.

Several ground and space-borne telescopes in the radio, millimeter, optical, and X-ray bands observed BL Lac during this IXPE observation; see the Appendix, where details about the instruments, observing dates, and data reduction and analysis are provided. Using several telescopes across the world, we were able to achieve nearly uninterrupted optical polarization coverage throughout the IXPE observation. No significant X-ray polarization was detected in the 2-8 keV band, similar to the previous IXPE observations. We are able to place a 99.73% (3σ) confidence level upper-limit on the polarization degree of $\Pi_X < 7.4\%$ in that band (2-8 keV), see the Appendix. A recent analysis of our IXPE data (Mondal et al. 2025) also resulted in a non detection of the linear polarization. Mondal et al. (2025) gave a less constraining upper limit of $\Pi_X < 7.5\%$ at 99% confidence level. Our $\Pi_X < 7.4\%$ upper limit therefore constitutes the most stringent constraint on the polarization degree from an LSP/ISP blazar, and almost a factor of two improvement over previous IXPE observations of BL Lac. The presence of variability in the polarization direction would lead to incoherent averaging of the polarization vectors, partially canceling any polarization signal (e.g., Di Gesu et al. 2023). We tested for such variability of the X-ray polarization using four independent methodologies; see
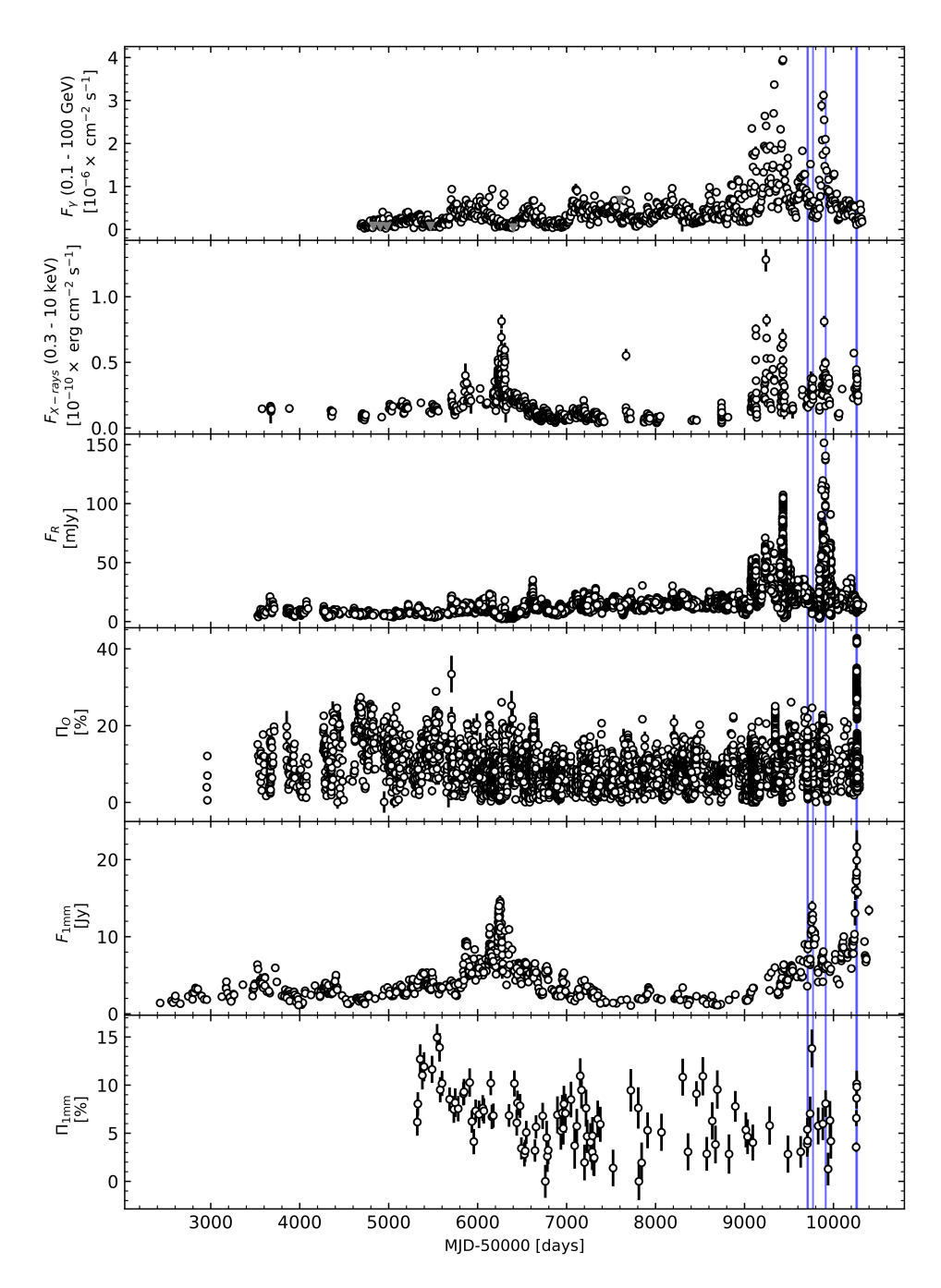
Figure 2. Historical light curves of BL Lacertae between 2005 and 2024. From top to bottom: γ-ray photon flux between 0.1 GeV and 100 GeV (flux points with black open markers and upper limits with grey markers), X-ray flux between 0.3 and 10 keV, optical R-band flux density, optical R-band polarization degree (%), radio 1 mm flux density, and radio 1 mm polarization degree. Blue vertical lines indicate the previous and current IXPE observations of BL Lacertae. A description of the origin of the data in this figure is provided in the Appendix.

Section B.4: Time-binned IXPE polarization analysis. None of the tests provided high significance ($\gg 3\sigma$) evidence of rotation of the polarization angle; see the Appendix.

During the IXPE observation, the measured optical polarization reached a maximum level of $\Pi_O = 47.5 \pm 0.4\%$ (Fig. 1). This is the most highly polarized state ever reported for BL Lac, and rivals the maximum measured in any blazar (e.g., Smith 2017). The short millimeter wavelength (1.3 mm, 225.5 GHz) polarization increased to $\Pi_{mm} \sim 10\%$, following a similar trend as at optical wavelengths, both in polarization degree and angle. During the
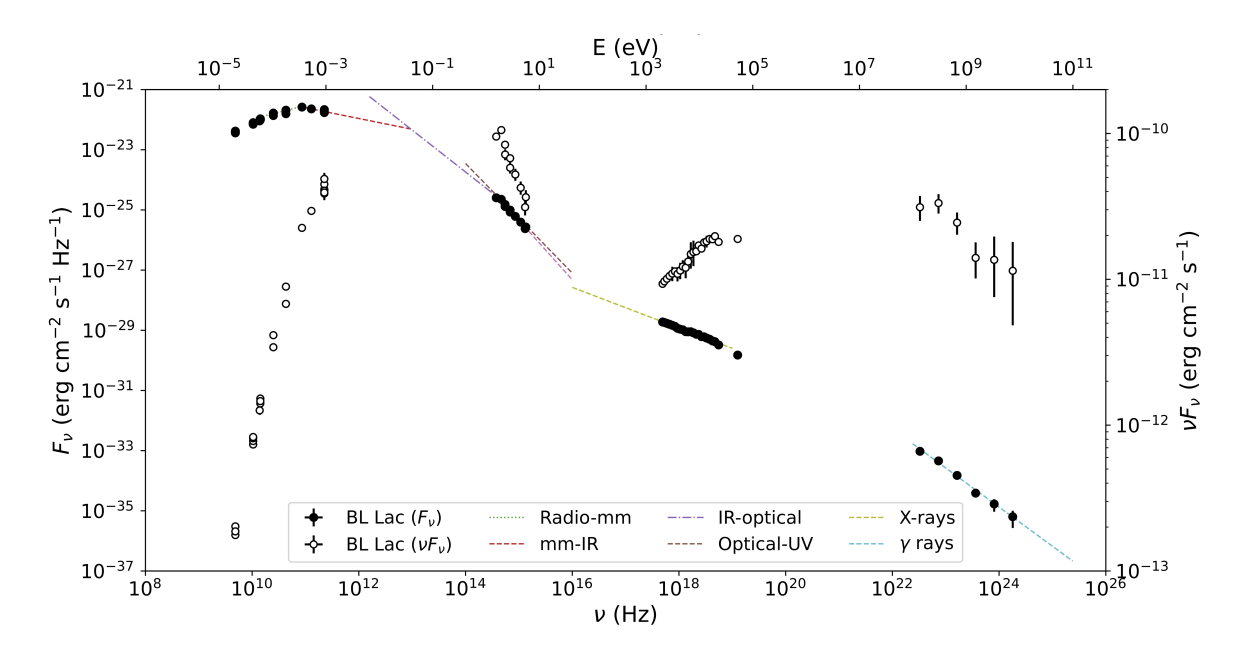
Figure 3. Flux density F_ν (black markers, in units of erg cm^{-2} s^{-1} Hz^{-1}) at frequency ν (Hz) and SED (open markers, in units of erg cm^{-2} s^{-1}) of BL Lac from radio to γ-ray frequencies during the time span of the IXPE observations. The different colored lines correspond to the power-law fits used for the estimation of the spectral indices (α, where $F_\nu \propto \nu^\alpha$) of each band, as specified in the legend and in the Appendix, Table 4.

Table 1. Summary of the multiwavelength polarization expectations for different X-ray emission scenarios outlined in the text.

Model	X-ray polarization degree	X-ray polarization variability
single-zone leptonic (EC)	Unpolarized	—
single-zone leptonic (SSC)	$0.5 \times \Pi_O$	similar to optical
energy-stratified/multizone leptonic (SSC)	$\leq 0.3 \times \Pi_O$	similar to millimeter
single-zone hadronic	$\approx \Pi_O$	less variable than optical
energy-stratified/multizone hadronic (flare)	$\approx \Pi_O$	less variable than optical
energy-stratified/multizone hadronic (non-flare)	$\approx \Pi_{mm}$	similar to millimeter

optical polarization flare, we also observed total flux brightening in the mm, optical, and X-ray bands (see Fig. 4 and the Appendix). The infrared (IR) to optical and γ-ray spectral indices (-1.39 ± 0.01 and -1.31 ± 0.08, respectively) displayed similar values during the IXPE pointing, while the X-ray spectral index (-0.68 ± 0.01) lay between the millimeter-IR (-0.36 ± 0.08) and the IR-optical (-1.39 ± 0.01) values; see Fig. 3 and subsection Broad-band spectral index analysis in the Appendix. The latter implies that the IR spectral index matches the X-ray slope over part of the IR wavelength range.

3. DISCUSSION

The origin of the high-energy bump of the SED of blazar jets depends on the nature of the radiating particles. In the leptonic scenario, electrons (and also positrons, if any) dominate the emission via Compton scattering. For isotropic seed photons, radiation scattered by relativistic leptons in the jet is unpolarized (Bonometto & Saggion 1973). For an internal photon field (i.e., synchrotron self-Compton, SSC), if the emission is produced in a single localized region in the jet, the polarization of scattered radiation would be ~ 0.5 times that of the seed photon field (Nagirner & Poutanen 1993; Poutanen 1994; Krawczynski 2012), and the spectral index of the seed photon field should equal that of the scattered photon population. If there is energy stratification in the emission region or there are multiple emission regions, the polarization degree would be lowered by a factor of ~ 3 or even more (Liodakis et al. 2019; Peirson & Romani 2019; Zhang et al. 2024). It is also possible that energetic photons are produced by scattering by a beam of

cold electrons in relativistic bulk motion. This would produce higher polarization in the X-ray than in the optical bands (Begelman & Sikora 1987). This scenario is rejected by our observations, and also by previous IXPE results (Middei et al. 2023; Peirson et al. 2023; Marshall et al. 2023; Kouch et al. 2024a).

In the hadronic scenario, protons can contribute to the high-energy radiation through (i) direct proton-synchrotron radiation or (ii) a photo-pair process that produces electrons and positrons (and other, short-lived, charged leptons), which in turn emit synchrotron radiation. If the process is localized in a single emission region, the X-ray polarization would be comparable to that in the optical bands (Zhang & Böttcher 2013; Paliya et al. 2018; Zhang et al. 2019). Even if there is energy stratification in the emission region or there are multiple emission regions, the polarization during a simultaneous multiwavelength flare (i.e., with no pronounced cross-frequency time delays owing to radiative energy losses) is expected to be similar to the case of a single emission region (Zhang et al. 2024). If the contributing protons have a spatially extended distribution inside the jet, the X-ray polarization of the emission from the protons would be comparable to the millimeter polarization (Zhang et al. 2024). The expected polarization of the models is summarized in Table 1.

Given that protons have much longer cooling timescales than electrons, the X-ray polarization for proton emission processes should show less prominent variability than the optical polarization, which is due to relativistic electrons that lose energy more rapidly through emission of radiation (Paliya et al. 2018; Zhang et al. 2019). As we do not observe significant variability in the millimeter or optical polarization angle, no significant depolarization is expected when averaging over the duration of the IXPE observation. We find that both the millimeter and optical polarization fractions are higher than the 3σ X-ray upper limit during a significantly elevated total flux emission state at radio, optical, and X-ray bands. The optical polarization is > 6 times higher than the X-ray upper limit, hence we can reject all of the single-zone hadronic models. Based on the expectations of X-ray polarization at least as strong as that at optical or millimeter wavelengths, the multi-region hadronic scenario can be confidently rejected as well.

The average (over the IXPE exposure) optical polarization of 25%, which is a factor of ~ 3 lower than that corresponding to a uniform magnetic field, can result from ~ 9 turbulent cells (e.g., Marscher & Jorstad 2022). In an energy-stratified shock model, the polarization should depend on frequency as $\nu^{-1/2}$ (Marscher & Jorstad 2022). The expected polarization of the energy-stratified/multi-zone SSC and external Compton (scattering of seed photons originating outside of the jet) emission scenarios is then between 0 and 5%. This is consistent with the IXPE upper limit. Focusing on the optical polarization peak (MJD 60261-60262.75), for an average optical polarization degree $\Pi_O = 40\%$, the SSC expectation is 14% (see Zhang et al. 2024). Repeating the IXPE analysis within the time interval near the peak yields a 3σ upper limit of $<21\%$, again consistent with the SSC scenario.

The optical polarization degree Π_o observed during the IXPE observation showed a dramatic increase from an initially low level, followed by a rapid decay, which provides direct evidence for a reconfiguration of global magnetic fields in the jet at ~ 1 pc from the central engine. Here we suggest a "magnetic spring" scenario as the primary mechanism accounting for this drastic variation in polarization. Before the rise in optical polarization, Π_o was $\sim 5\%$, with the polarization angle aligned along the jet direction. As jets typically possess both poloidal and toroidal magnetic components, this suggests that the toroidal magnetic field was comparable to, or weaker than, poloidal and/or turbulent magnetic field components. At its peak ($\Pi_o = 47.5 \pm 0.4\%$), the polarization angle remained aligned with the jet direction, indicating that the toroidal component became at least 2.5 times stronger than the poloidal and/or turbulent components. We suggest that this could be caused by an injection of a magnetic "spring" with a dominant toroidal configuration, embedded in the jet plasma flowing outward from the central engine. Such an injection could arise from a magnetic eruption from a magnetically arrested disk (e.g., Ripperda et al. 2022) and it continues into the relativistic jet (Yang et al. 2024). Subsequently, the rise and fall of the optical polarization over ~ 2 weeks imply a rapid relaxation of the injected toroidal component in a compact region (~ 0.1 pc) such that the toroidal component eventually becomes comparable to the poloidal components, as could occur through a kink instability in the jet (Guan et al. 2014; Barniol Duran et al. 2017). The relaxation time of the toroidal component via kink instabilities is on the order of the Alfvén crossing time, which is about a week for typical blazars (Zhang et al. 2017). The observed approximately symmetric rise and fall in Π_o suggest that magnetic fields in this jet play an active role in restoring their configurations, different from a low-magnetization plasma environment where the rise and fall in Π_o are not expected to be symmetric (Zhang et al. 2016). With a kink instability, some of the toroidal magnetic field can be converted into the poloidal component, reducing Π_o and contributing to the curved jet morphology observed in VLBA images (Figure 9).

The injection of a toroidally-dominated magnetic spring can also account for the multiwavelength flaring behavior. This injection leads to a sudden increase of the total magnetic field strength, producing the historically high flare in the mm-band. This flare occurs near the low-energy spectral turnover, with synchrotron radiation emitted by relatively low-energy electrons (compared to those emitting at optical and X-ray wavelengths), whose cooling times are on the order of years. The fact that the mm-band polarization degree does not rise as much as the optical band is consistent with the scenario that mm-band and lower energy emission comes from a much larger volume, subject to contributions from many local magnetic field configurations and probably turbulent magnetic fields in the jet, as well as synchrotron self-absorption effects. This is consistent with the energy stratified picture reported in previous X-ray polarization observations of HSPs (Marscher & Gear 1985; Liodakis et al. 2022; Di Gesu et al. 2023; Middei et al. 2023; Kouch et al. 2024b). This is also supported by a BL Lac analysis made by Mondal et al. (2025) on a similar time span using a less populated dataset without optical and radio polarization information. Meanwhile, the optical band, near the high-energy turnover of the synchrotron SED, shows suppressed flaring due to enhanced synchrotron cooling (and therefore less efficient acceleration) of high-energy electrons. This is consistent with the observed softening of the optical spectral index (Table 4). Similarly, there is no prominent increase in γ-ray flux, since it is produced mainly by Compton scattering by the same electrons that emit optical synchrotron radiation.

4. CONCLUSION

Our results unambiguously reject single-zone hadronic processes and multizone/energy stratified hadronic scenarios in BL Lac. Instead, they favor a scenario where X-ray emission is dominated by Compton-scattered emission from relativistic electrons in a region with gradients in the maximum electron energy. This could be realized where electrons are accelerated in a fresh plasma blob threaded by a magnetic spring dominated by a strong toroidal magnetic field in the parsec-scale region, beyond which electrons are subsequently advected downstream. While protons may occasionally play an important role in the emission from blazar jets, and their interactions in jets might be associated with neutrino detections, our polarization study implies that this is not the typical case. Our observations constitute the strongest test of X-ray emission processes in astrophysical jets so far, and the strongest evidence against relativistic protons dominating the X-ray emission in blazars. Our study also demonstrates the rich potential of multiwavelength total flux and polarimetric monitoring campaigns that include X-ray polarimetry and ultra-high angular resolution VLBI observations to resolve the long-standing question of the role that relativistic protons play in blazar jets.

Software: HEASoft (Nasa High Energy Astrophysics Science Archive Research Center (Heasarc) 2014), FTOOLS (Blackburn 1995), IOP4 (Escudero Pedrosa et al. 2024a,b), AIPS[1], DIFMAP (Shepherd 1997), GILDAS[2]

APPENDIX

The IXPE observation of BL Lac presented here was accompanied by contemporaneous observations from several ground and space-based facilities. We give a short description for each of those facilities below. More details of the observations and data reduction, including information on the individual telescopes, can be found in Liodakis et al. (2022); Di Gesu et al. (2022); Peirson et al. (2023); Middei et al. (2023); Kouch et al. (2024b).

A. *FERMI*-LAT γ-RAY DATA

Data from the pair-conversion Large Area Telescope (LAT) on board the *Fermi* satellite are included in this work. This telescope monitors the γ-ray sky every three hours in the energy range of 20 MeV to $\sim$2 TeV, with sensitivity highest in the 0.1–200 GeV range (Atwood et al. 2009). We have retrieved the publicly available BL Lac light curve from the *Fermi*-LAT public Light Curve Repository (LCR[3], see Abdollahi et al. 2023). This database contains the light curves of all variable sources in the 4FGL-DR2 catalogue (Abdollahi et al. 2020; Ballet et al. 2020), which includes sources with a variability index >21.6 (see Table 12 in Abdollahi et al. 2020). We refer to Abdollahi et al. (2023) for a detailed discussion on the automatic unbinned likelihood analysis adopted by the LCR for computing the light curves. Here, we have used the 3-day binned light curve with a freely varying spectral slope in each bin. Figure 2 shows the γ-ray lightcurve compiled since the beginning of operations of *Fermi*. The light curve shows that the γ-ray flux level of the source during the IXPE observation reported here was low to moderate.

We have derived the γ-ray portion of the SED and spectrum of BL Lac during the IXPE observation by retrieving and analyzing the data from the LAT Data Server[4], plus an extra ± 15 days around it, i.e., between 2023 October 23 and 2023 December 3. This extended time window was selected owing to the relatively faint and stable γ-ray emission of the source in the period that is strictly simultaneous with IXPE observations, which would lead only to upper limits over that period. We have selected and analyzed all of the Pass8 `P8R3_source` events between 100 MeV and 300 GeV with version 1.2.23 of the standard software FERMITOOLS. A cut of $90°$ in zenith angle was applied to minimize the contamination from the limb of the Earth. The recommended Galactic diffuse emission model and isotropic component for the event selection and analysis performed here were employed[5].

In order to obtain a model describing all of the relevant sources in the field, a binned likelihood analysis was performed on 1 year of LAT data (January 2019 to January 2020). We included all sources contained in the defined region-of-interest (ROI) near BL Lac, plus those located within an additional annular region of $10°$ radius. For inclusion into the final model, the spectral parameters and flux normalization of all sources within the ROI were left as free parameters. For the sources within the annular region, these parameters were fixed to those from the 4FGL-DR2 catalogue. The normalization of the diffuse components were also left as free parameters. In the convergence iteration, all sources with a test statistic (TS) <4 (approximately 2σ significance) were removed from the final model.

Finally, we have also extracted the γ-ray spectrum and SED of BL Lac in the aforementioned time window. We used a binned likelihood analysis to model each bin of the SED with a power-law spectral model. The LAT catalogues show a significant preference for a log-parabolic spectral shape after averaging more than 14 years of data. However, due to the short interval considered here, we do not accumulate enough statistics to observe a preference for a curved spectrum over the simpler power law model. Hence, we adopted the latter for the SED estimated here, obtaining a power-law spectrum with an index $\alpha = -2.31 \pm 0.08$.

B. X-RAY DATA

B.1. *IXPE observation and data reduction*

BL Lac was observed by IXPE's three Detector Units (DUs) from 2023-11-07 00:44:08 to 2023-11-17 19:48:05 for a total exposure time of $\sim$515 ks. The I, Q, and U spectra for each of the three DUs of IXPE were computed using the

---

[1] http://www.aips.nrao.edu/aipsdoc.html

[2] https://www.iram.fr/IRAMFR/GILDAS/

[3] https://fermi.gsfc.nasa.gov/ssc/data/access/lat/LightCurveRepository/about.html

[4] https://fermi.gsfc.nasa.gov/ssc/data/access/lat/

[5] https://fermi.gsfc.nasa.gov/ssc/data/access/lat/BackgroundModels.html

Table 2. Log of X-ray observations related to the IXPE pointings of BL Lac.

Observatory	Obs. ID	Obs. date	Net exp.
		yyyy-mm-dd	ks
IXPE	02009701	2023/11/07-17	~ 515
NuSTAR	80901639002	2023/11/13-14	~ 20
XMM-Newton	0902112601	2023/11/17	~ 5

software IXPEOBSSIM (v. 31.0.1, Pesce-Rollins et al. 2019; Baldini et al. 2022) and adopting the background rejection prescriptions by Di Marco et al. (2023). The spectra were computed to enable the use of the weighted analysis method (Di Marco et al. 2022). The Stokes I, Q, and U spectra were extracted using a circular region with radius=$0.95'$ centered on BL Lac. The background was derived using an annular region with $r_{\mathrm{in(out)}}$=$1.2'(3.5')$. These choices have been shown to enhance the sensitivity to polarization, as discussed by Di Marco et al. (2023). The resulting I Stokes spectra were rebinned, requiring each energy bin to have a signal-to-noise ratio greater than 7. A uniform binning of 280 eV was then adopted for the Q and U Stokes spectra.

B.2. *Swift, XMM-Newton and NuSTAR observations and data reduction*

The IXPE observation of BL Lac was coordinated with different X-ray observatories: XMM-Newton (Jansen et al. 2001), the Neil Gehrels Swift observatory (Swift, Gehrels et al. 2004), and the Nuclear Spectroscopic Telescope Array (NuSTAR, Harrison et al. 2013). This joint effort allowed us to monitor the source variability and derive the intrinsic spectral shape of the source below and above the IXPE 2-8 keV bandpass.

The X-ray Telescope (XRT) on *Swift* operates in the 0.2-10 keV energy band and has a high spatial resolution of $18''$. Both the XRT and UltraViolet and Optical Telescope (UVOT) operate simultaneously to enable concurrent observations in different electromagnetic bands (Roming et al. 2005; Burrows et al. 2005). We retrieved the reducedX-ray, UV, and optical data from the *Swift* public mirror archive [6] of the Space Science Data Center (SSDC) at the Italian Space Agency (ASI). *Swift*-XRT observed BL Lac in Photon Counting (PC) readout mode. The data were first reprocessed locally with the XRTDAS software package (version v3.7.0), developed by the ASI-SSDC and included in the NASA-HEASARC HEASoft package[7] (version v6.31.1). Standard calibration and filtering processing steps were adopted and the calibration files available from the *Swift*-XRT CALDB (version 20220803) were used. The science products were extracted using a circle of 20 pixels ($47''$) radius centered on the target source, while the background was derived from a nearby circular region with a radius of 40 pixels. All the spectra were subsequently binned with the grppha tool of the FTOOLS package[8] requiring each bin to have a minimum of 5 counts, and then modeled using the XSPEC software package[9] while adopting a single power-law model with foreground photoelectric absorption from gas in our Galaxy. In Figure 4 we show the temporal behavior of the power-law slope (photon index), soft and hard fluxes (0.5-2 and 2-10 keV, respectively) and hardness ratios of BL Lac.

The UVOT on board Swift is capable of observations in the $[170, 600]$ nm band performed simultaneously with Swift-XRT. In our case, the UVOT pointed at BL Lac with filters V 5468Å, B 4392Å, U 3465Å, UVW1 2600Å, UVM2 2246Å, UVW2 1928Å. We derived the photometric points for each filter for the different observations using the standard tools within an automated reduction procedure. We adopted two regions, a circular one centred on the source (radius = $2''$) for estimating the counts from the target, while a concentric annulus (Δradius = $7''$), free of any other sources or spurious detection, was used to determine the background. We show the returned count rates for the UVOT filters, uncorrected for Galactic or intrinsic reddening, in Figure 4.

XMM-Newton, which is sensitive to soft X-rays, briefly observed BL Lac for about 5 ks, from 2023-11-17 12:21:37 to 2023-11-17 19:08:46. The satellite's EPIC-pn camera (Strüder et al. 2001) observed BL Lac in Small Window mode, with the medium filter applied. Data were processed with the standard XMM-Newton Science Analysis System (SAS v21 Gabriel et al. 2004). Source extraction radii and screening for high-background intervals were determined through an iterative process (Piconcelli et al. 2004) that maximizes the signal-to-noise ratio. The background was extracted from circular regions with a radius of $50''$, and the same shape centered on BL Lac was adopted for science products.

---

[6] Available at https://swift.ssdc.asi.it/

[7] Available at https://heasarc.gsfc.nasa.gov/docs/software/heasoft/

[8] Available at https://heasarc.gsfc.nasa.gov/ftools/

[9] Available at https://heasarc.gsfc.nasa.gov/xanadu/xspec/
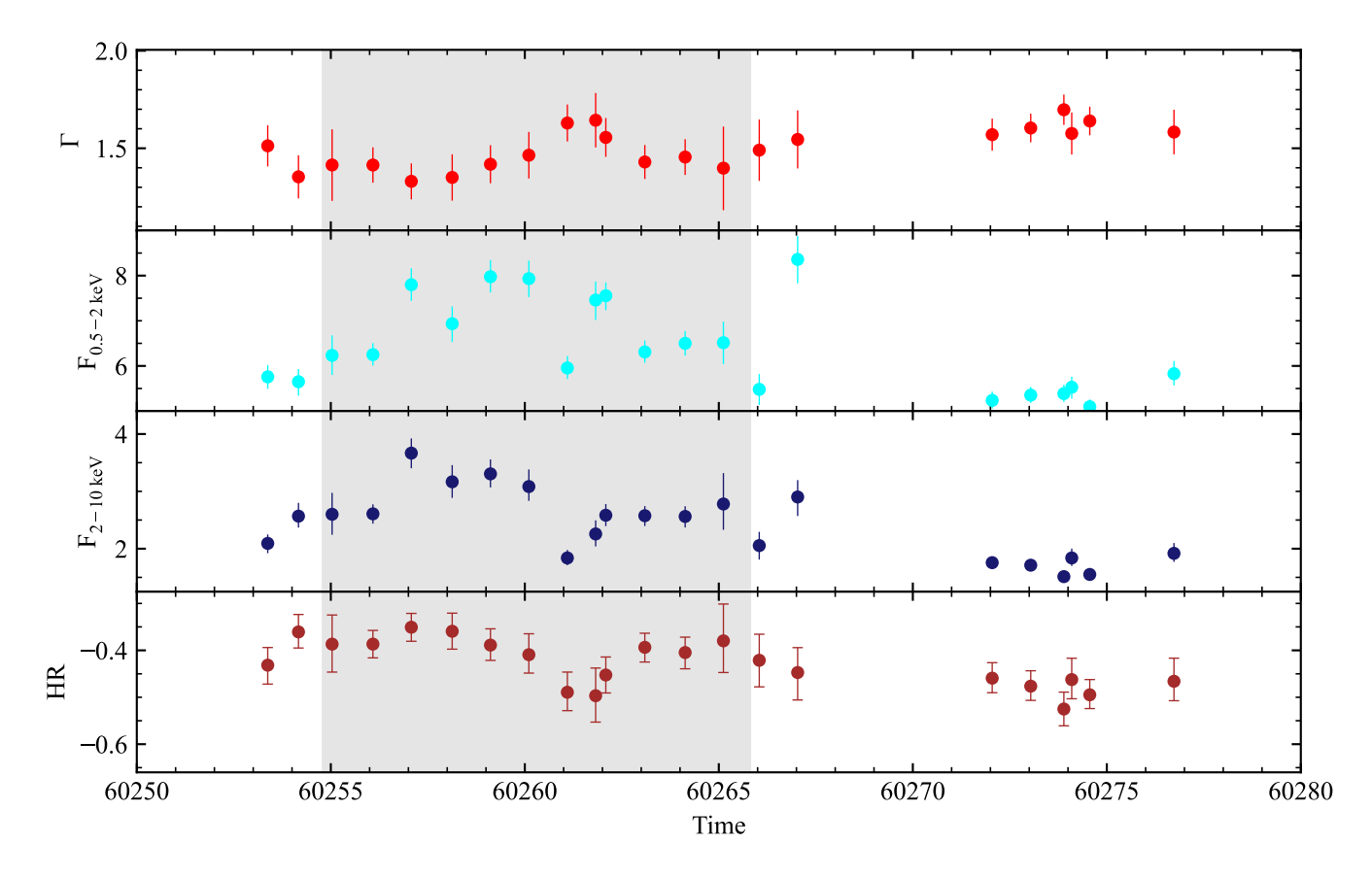
Figure 4. Results of the Swift-XRT monitoring campaign of BL Lac. Fluxes $F_{0.5-2 \text{ keV}}$, and $F_{2-10 \text{ keV}}$ are displayed in units of 10^{-12} erg cm^{-2} s^{-1} and 10^{-11} erg cm^{-2} s^{-1}, respectively. The label "HR" stands for hardness ratio, which we define as $(F_{2-10 \text{ keV}}-F_{0.5-2 \text{ keV}})/(F_{2-10 \text{ keV}}+F_{0.5-2 \text{ keV}})$. Gray shaded areas mark the duration of the IXPE pointing.

The resulting third-level products were grouped by requiring each bin to contain at least 30 counts, and not to over-sample the spectral resolution by a factor larger than 3. The net count rate was less than the maximum allowed limit of 50 cts s^{-1} to avoid deteriorated response due to photon pile-up for EPIC-pn observations in Small Window mode (e.g. Jethwa et al. 2015). We further assessed the potential impact of pile-up in the XMM-Newton observation by means of the *epatplot* task, a standard SAS command devoted to checking for any pile-up affecting the data, and we found it to be negligible.

NuSTAR observed BL Lac simultaneously with IXPE for a total of ∼20 ks from 2023-11-13 16:11:09 to 2023-11-14 02:51:09. The FPMA/B instruments carried on its focal plane operate in the 3-79 keV range, thereby providing unique broadband data. Science products of BL Lac were obtained by employing the NuSTARDAS software, also developed by the ASI-SSDC and included in the NASA-HEASARC HEASoft package, and the latest calibration data files CALDB (version 20220510). We used a circular region (radius r∼70") centered on BL Lac to extract both the FMPA and FPMB spectra. The same sized region, but located on a black area of the detectors, was used to extract the background. The ancillary and response matrices were computed at this stage, and we grouped the spectra via the grppha standard command in order to have at least 30 counts per bin.

B.3. *Time-averaged spectro-polarimetric analysis*

Our search for a polarized X-ray signal from BL Lac relied on a spectro-polarimetric analysis in which we simultaneously modeled the IXPE, XMM-Newton, and NuSTAR spectra. We proceeded in the manner of Middei et al. (2023), where a similar dataset was analysed. In particular, we tested a simple phenomenological model in *XSPEC* that can be written as tbabs×const×po×polconst. The first component accounts for the column density through gas in our Galaxy and whatever additional hydrogen might intercept our line of sight (e.g. Bania et al. 1991; Madejski et al. 1999; Middei et al. 2023). The constant is used for the inter-calibration of the different telescopes, and the power law

Table 3. Best-fit parameters for the joint X-ray observations. All uncertainties are quoted at 68% confidence level for one parameter of interest. The 2-8 keV flux is estimated from the IXPE data, while fluxes in the 0.5-2 and 2-10 keV bands are derived from the XMM-Newton data.

component	parameter	value	units
polconst	Π_X	< 7.4% (C.L. 99.73%)	-
	Ψ_X	-	-
tbabs	N_H	2.45±0.07	$\times 10^{21}$ cm^{-2}
powerlaw	Γ	1.87±0.01	-
	Norm	6.72 ± 0.01	$\times 10^{-3}$ photons keV^{-1} cm^{-2} s^{-1}
const	k_{DU2}	0.97 ± 0.01	-
const	k_{DU3}	0.88 ± 0.01	-
const	k_{pn}	0.78 ± 0.01	-
const	k_{FPMA}	1.07 ± 0.02	-
const	k_{FPMB}	1.11 ± 0.02	-
$F_{2-8\ keV}$		1.75 ± 0.01	$\times 10^{-11}$ erg cm^{-2} s^{-1}
$F_{2-10\ keV}$		1.60 ± 0.02	$\times 10^{-11}$ erg cm^{-2} s^{-1}
$F_{0.5-2\ keV}$		6.45 ± 0.05	$\times 10^{-12}$ erg cm^{-2} s^{-1}

describes the X-ray continuum spectrum. The polarization signal is encoded in the Q and U Stokes spectra, and is determined from the multiplicative component *polconst*, which assumes the X-ray polarized signal to be constant in the IXPE operating band.

The spectro-polarimetric fit is performed by computing the photon index of the continuum and its normalisation, the polarization degree Π_X and polarization angle Ψ_X, and five constants accounting for the DU1, DU2 and DU3 detector units of IXPE, the EPIC-pn camera, and the FPMA/B modules of NuSTAR. These simple steps returned a fit with χ^2/d.o.f.=1039/932. Similarly to the discussion in Middei et al. (2023), the observed column density exceeds the Galactic value and the EPIC-pn spectrum shows bump-like residuals around 0.7 keV that may be due to some additional spectral component. We investigated the possible origin of these bump-like residuals by examining whether the unmodeled data could be attributed to a steep upper tail of the synchrotron spectrum entering the XMM-Newton band pass. To test this, we replaced the Gaussian line by a second power law for which the photon index and the normalization were fitted. However, this attempt returned a poorer fit with χ^2/d.o.f.=638/553. As a second test, we replaced the two power laws with a broken power law (BKNPO in XSPEC notation) and fit the two Γ the break energy and the normalization of the power law. This second attempt yielded to a better fit (χ^2 =556 for 553 d.o.f.) but the very flat soft spectral shape predicted by this model ($\Gamma_{soft} \sim 0.2$) is not consistent with the hypothesis of a soft synchrotron component extending up to ~2 keV. We thus proceeded as in Middei et al. (2023) and updated our fitting model to include an unpolarized *apec* component that could explain the excess in the soft X-ray band as emission from hot diffuse plasma. The addition of this Gaussian component is beneficial in terms of χ^2, as the statistic improved by $\Delta\chi^2$/Δd.o.f.= $-70/-2$. This best-fitting model is shown in Figure 5, and the inferred quantities are reported in Table 3. Our analysis reveals that the X-ray spectrum of BL Lac beyond ~ 2 keV was well represented by a power law with photon index $\Gamma = 1.87\pm0.01$. The density of the absorbing column, although exceeding the Galactic value, was found to be N_H=2.45±0.05$\times 10^{21}$ cm^{-2}, in agreement with previous studies (e.g. Weaver et al. 2020). Below the IXPE bandpass, the EPIC-pn spectrum seems compatible with emission from hot gas ($kT = 0.38\pm0.04$ keV), although a physical origin for such a hot gas is unknown and requires further study.

According to our analysis, no significant polarization of BL Lac was measured by IXPE during the campaign. The 3σ (99.73% confidence level) upper limit to the polarization degree is $\Pi_X^{3\sigma}$ <7.4%, while the corresponding value at 99% confidence level is Π_X^{99} <6.6%. No indications of significant polarization could be found by altering the energy range. Finally, all cross-normalization constants are in agreement with each other within ~20%.

B.4. *Time-binned IXPE polarization analysis*

We examined polarization variability over time and energy using a χ^2 test by dividing the entire observation into specific time and energy bins, as described in Kim et al. (2024). The χ^2 analysis was performed to estimate the null hypothesis probability (P_{Null}) of a constant model fit to the time-averaged q and u values of each bin obtained from
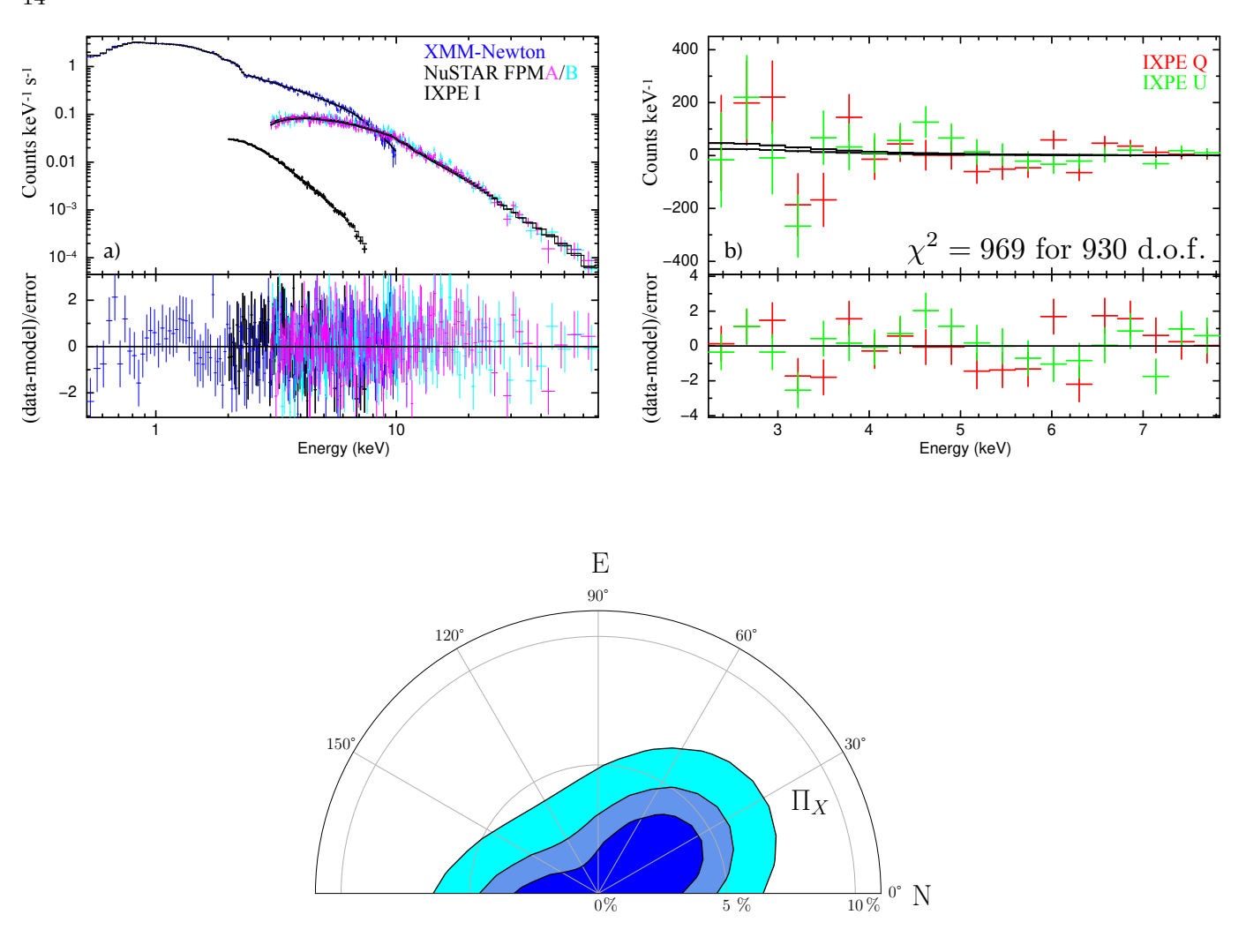
Figure 5. Top panels: Best fit to the IXPE, XMM-Newton, and NuSTAR data and corresponding residuals. On the left, the model $tbabs \times const \times polconst \times po$ fitting the I Stokes spectra is shown, while the right panel displays the best fit Q and U Stokes spectra. Bottom panel: confidence regions corresponding to 68%, 90%, and 99% uncertainties derived using the full IXPE 2-8 keV data.

the independent spectral modeling analysis. In the case of time variability, we estimated the time-averaged q and u values by dividing the entire observation period into specific sub-periods after dividing the data into two to 15 bins (e.g., 2 bins = 515ks/2 bins = 258ks per bin). To test for energy dependence, we divided the entire energy band (2-8 keV) into smaller energy bins, such as two energy bins (2-4 and 4-8 keV), three (2-4, 4-6, and 6-8 keV), and so on (up to 12). Figure 6 illustrates the calculated P_{Null} of q and u in percentage units for all of the different time binning cases. We found no statistically significant change in polarization when dividing the data into narrower time or energy ranges, with a probability higher than the 1% threshold in all cases.

We furthermore performed a study of the change in polarization over time. The data set was divided into equal intervals, and the polarimetric analysis was performed on each of them. Several interval durations were tested and a compatible result was obtained in each case. As a trade-off, we show the division in 6 time bins that provide higher time resolution and reasonable statistics in each time bin. We treated the background as in the time-averaged analysis and, as before, considered a weighted method. We used both a spectro-polarimetric analysis and the model-independent analysis described in Kislat et al. (2015). In the former case, we tested a simple phenomenological XSPEC model
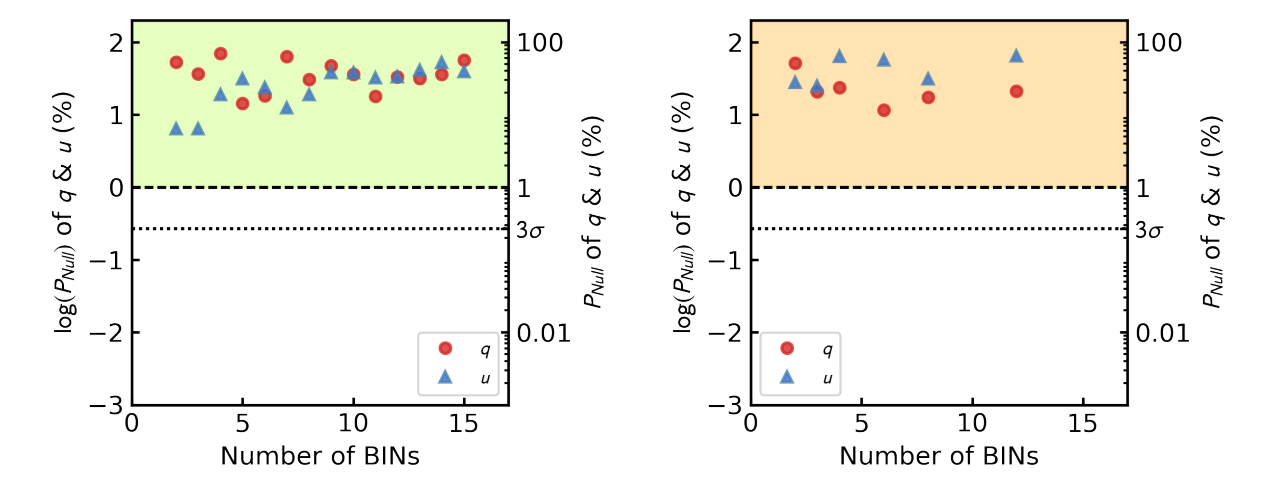
Figure 6. Null hypothesis probability of a constant model of the q (red) and u (blue) Stokes parameters for different time (left panel) and energy (right panel) bins. The green and orange shaded areas indicate that the null hypothesis probability is above the 1% threshold level. The black dashed and dotted lines located in the middle of each panel represent 1% and 3σ (0.27%) probability, respectively. The left and right vertical axes of each panel correspond to the probability values in logarithmic and linear scales in percentage, respectively.

that can be written as `tbabs×constant×pow×polconst`. In the latter, we applied the same method as for the time-averaged analysis. Several statistical tests were applied; the unpolarized model could not be rejected above the $\sim 3\,\sigma$ level in any bin or under any condition. Given the current sensitivity, no significant polarization detection can be therefore claimed. We have also performed several tests to look for energy dependence of the polarization. For this purpose, we tested the spectral model with *pollin* in XSPEC for each time bin. No significant energy dependence of the polarization was found.

Finally, because rotation of the EVPA during the IXPE observations could affect the measurement of the polarization degree, we have also checked the data for such a rotation. Using a 1-D test for EVPA rotation (Di Gesu et al. 2023) we found evidence at 99.5% confidence for a rotation of $12\pm3.5°$/day in the 2-8 keV band. Furthermore, dividing the data into four independent intervals and allowing for EVPA rotation in each interval, i, we find that the likelihood that the polarization is zero is rejected at 99.2% confidence. This method involves computing

$$\mathcal{S} = \sum_{i}^{\mathcal{N}}[\mathcal{S}_i(\hat{U}_i, \hat{u}_i, \hat{R}_i) - \mathcal{S}_i(0,0,0)] \tag{B1}$$

where $N = 4$, $\hat{q}_i$, $\hat{u}_i$, and $\hat{R}_i$ are the best fit parameters and S_i is the event-based log-likelihood computed for the interval i (Marshall 2024; Di Gesu et al. 2022). Thus, $\mathcal{S}$ is the 3-D likelihood ratio test of the hypothesis that the polarization is zero for all intervals and is distributed as χ^2 with $3N$ degrees of freedom. Finally, assuming $R = 12$ deg/day, the source polarization is 5.57 ± 1.75 %.

C. OPTICAL DATA

Optical observations covering the entirety of the IXPE exposure were obtained at the Belogradchik Observatory (R-band, Bachev et al. 2023), Calar Alto Observatory (CAFOS, R-band, Escudero Pedrosa et al. 2024b), Nordic Optical Telescope (ALFOSC, R-band, Nilsson et al. 2018), Liverpool Telescope (MOPTOP, BVR-bands, Shrestha et al. 2020), LX-200 photometry ($BVRI$-bands) and polarimetry (R-band), Perkins Telescope (PRISM, $BVRI$-bands, photometry and polarimetry, Jorstad et al. 2010), Sierra Nevada Observatory (DIPOL-1, R-band, Otero-Santos et al. 2024), and the Skinakas observatory (RoboPol, R-band, Ramaprakash et al. 2019). The CAFOS and DIPOL-1 observations were analyzed using IOP4 (Escudero Pedrosa et al. 2024a,b), while the RoboPol observations used the automatic pipeline described in Panopoulou et al. (2015); Blinov et al. (2021). The 40cm LX-200 telescope uses an imaging photo-polarimeter with a ST-7 camera and two Savart plates oriented $45°$ with respect to each other. The R-band polarization observations were corrected for interstellar and instrumental polarization using standard stars.
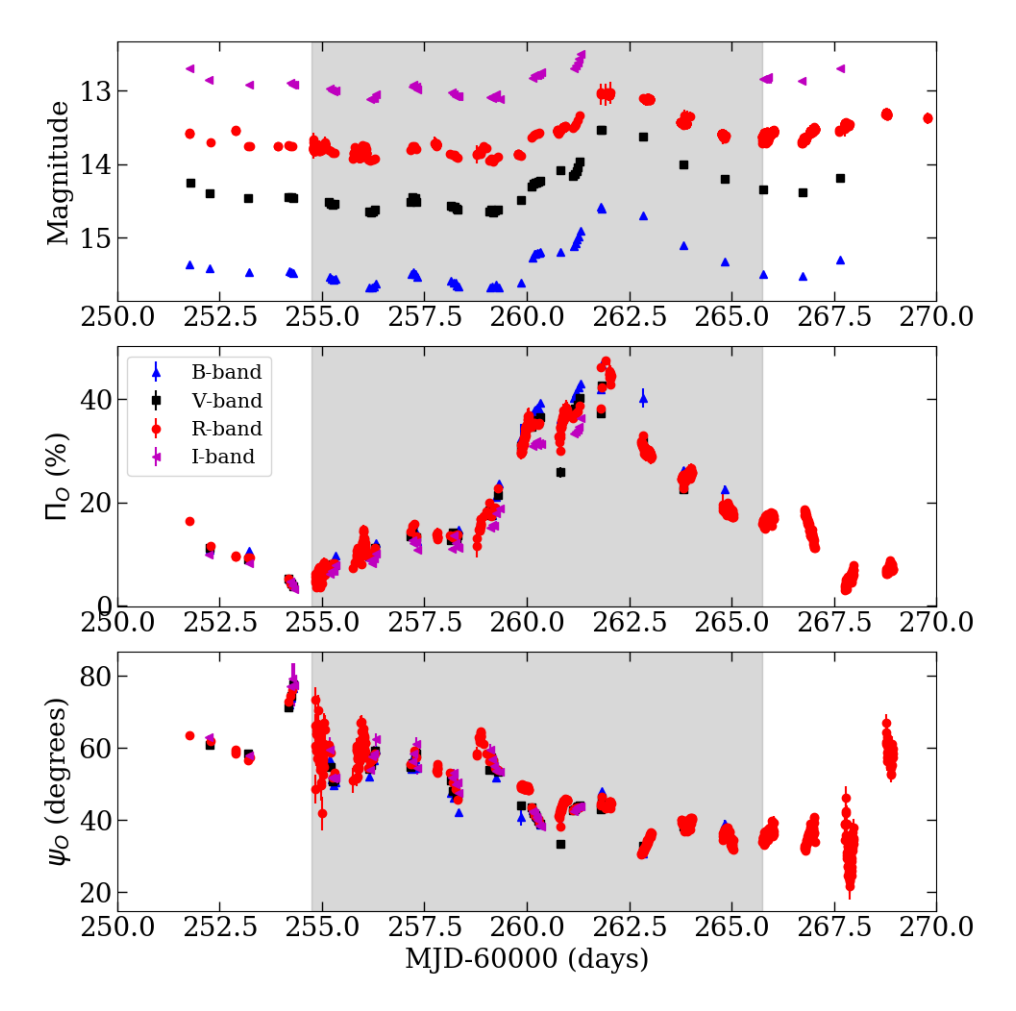
Figure 7. Optical polarization measurements during the IXPE observation. The top panel shows the brightness in magnitudes, the middle panel the polarization degree (%), and the bottom panel the polarization angle (degrees). The grey shaded area marks the duration of the IXPE observation. The different optical bands are marked with different symbols and colors as shown in the legend. The error bars correspond to the 68% (1σ) confidence interval.

In the case of BL Lac, as well as many other BL Lac type objects, the host galaxy contributes significantly to the total optical emission. This leads to dilution of the intrinsic polarization degree. To account for this effect, we use the host-galaxy light-distribution model from Nilsson et al. (2007) to estimate the contribution of the host galaxy to the flux density (in mJy) at the aperture used for the polarization analysis for each observatory. We then correct the observed polarization degree by subtracting the host flux density from the total flux density following Hovatta et al. (2016). Since we only have a model for the host galaxy in the R-band, only the R-band measurements have been corrected. In this case the correction is small, yielding a change of only 1–3%. Although we have not corrected the other optical bands, the brightness of a typical elliptical galaxy, as is the case for the host galaxy of BL Lac, falls sharply towards higher frequencies. The host correction in the B- and V-bands is typically negligible, while is it more significant in the I-band.

The optical polarization measurements are shown in Figure 7. We see achromatic variations in brightness and polarization properties. There is a high-amplitude outburst in polarization degree that coincides with the IXPE observation. The polarization degree starts at 4%, rises to 47.5%, then declines to 16% from the beginning to the end of the IXPE observation. This matches the highest polarization ever reported from a blazar (the previous record of $47.4 \pm 0.1\%$ was observed in PKS 1502+106, Smith 2017). At the same time, there is a less prominent flare in optical total flux. The polarization angle slowly drifts from 70° to 30° with a median of 45°, without any indications of large variations or rotations, as are often exhibited by BL Lac (e.g., Marscher et al. 2008; Blinov et al. 2018). This particular optical behavior of BL Lac will be studied in detail in a forthcoming publication.
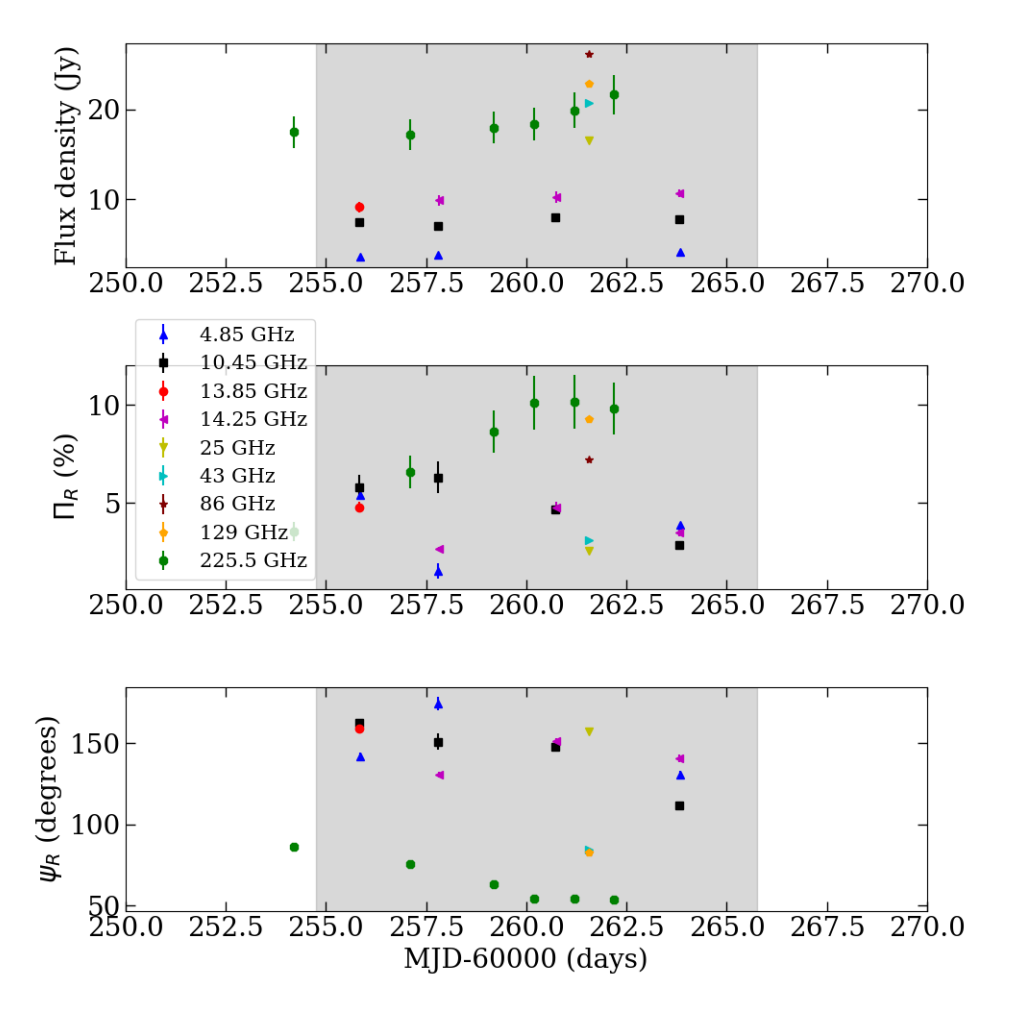
Figure 8. Short-millimetre-wavelength and radio polarization measurements during the IXPE observation. The top panel shows the flux density, the middle panel the polarization degree, and the bottom panel the polarization angle. The grey shaded area marks the duration of the IXPE observation. The different radio frequencies are marked with different symbols and colors as shown in the legend. The error bars correspond to the 68% (1σ) confidence level.

In order to provide a general overview of the behavior of BL Lac as compared to the one during this campaign, we have retrieved the historical photo-polarimetric R-band data from different observatories and databases. This includes measurements from Steward Observatory[10] (2008 to 2018, Smith et al. 2009), Skinakas Observatory (RoboPol[11], 2013 to 2017, Blinov et al. 2021), Calar Alto Observatory (CAFOS, Agudo et al. 2012) and Sierra Nevada Observatories (2007 to 2024), Perkins Telescope (2005 to 2023), LX-200 and AZT-8 telescopes (2005 to 2023), Nordic Optical Telescope (NOT, 2015 to 2020), and Tuorla blazar monitoring (KVA, 2003 to 2011), covering a period of more than 20 years. These data are shown in Figure 2. BL Lac is known for its remarkable variability across all bands, as exemplified by the past several bright flares, which reached optical magnitudes as bright as $R \sim 11$. Extreme flares have also been observed in X-rays and γ rays from this source. However, as shown by the variations in polarization degree over $\sim$20 years of monitoring, the nature of the event observed during the IXPE campaign is unique, reaching an all-time maximum polarization degree for any blazar. Interestingly, this feature coincides with a very low γ-ray emission state of BL Lac, as shown by the *Fermi*-LAT data, and with a relatively modest optical flare.

---

[10] http://james.as.arizona.edu/~psmith/Fermi

[11] https://robopol.physics.uoc.gr

Figure 9. Sequence of 43GHz VLBA images of BL Lac from the BEAM-ME program at 0.1 mas angular resolution. Contours represent total flux density from 0.01 Jy/beam (the lowest contour on every image) to 5.50 Jy/beam (the highest contour). There are 10 logarithmically equally spaced to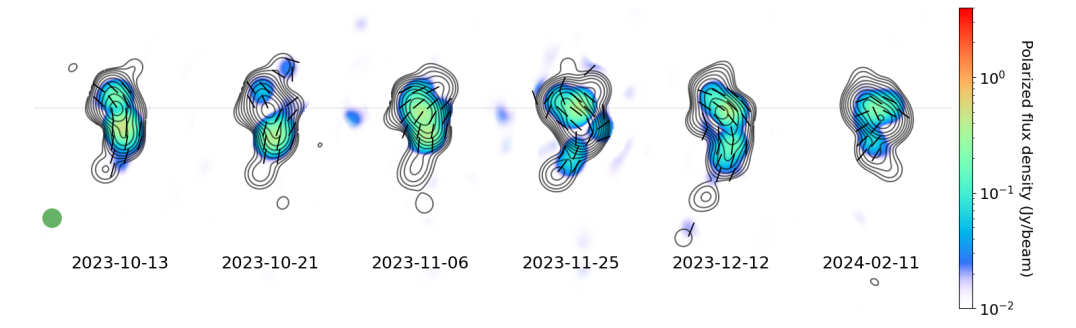tal flux contours from those minimum and maximum levels. The short sticks symbolize the direction of the electric vector polarization angle.

D. RADIO/MILLIMETRE DATA

BL Lac was observed from 4 GHz to 225.5 GHz , by the Effelsberg 100-m telescope as part of the Monitoring the Stokes Q, U, I and V Emission of AGN jets in Radio (QUIVER) program (4.8, 10.4, 13.8, 14.2 GHz, Kraus et al. 2003; Myserlis et al. 2018), the Korean VLBI Network (KVN, 25, 43, 86, 129 GHz, Kang et al. 2015), and by the Submillimeter Array (SMA) within the framework of the SMA Monitoring of AGNs with Polarization (SMAPOL) program (225.5 GHz, Ho et al. 2004; Marrone & Rao 2008; Primiani et al. 2016).

Figure 8 shows the contemporaneous radio observations. We find a similar behavior as in the optical observations. There is a brightening across frequencies that coincides with a sharp peak in the polarization degree, best visible in the better sampled 225.5 GHz observations. As usual in blazars (e.g., Agudo et al. 2018a), there is an increase of the polarization degree towards higher frequencies. At low radio frequencies (< 86 GHz) the polarization degree is in the range 1–6%. At higher frequencies (≥ 86 GHz) the polarization degree is between 6–10%. There is a similar trend in the polarization angle at 225.5 GHz, from $85°$ to $51°$, as we observe in the optical bands, although the polarization angle in the radio bands is higher than the optical. The jet axis on the plane of the sky is found to be $10° \pm 2°$ (Weaver et al. 2022) hence the radio and optical polarization angles wander by tens of degrees from the jet direction. (However, see the discussion of contemporaneous VLBA images below for a different viewpoint.)

We have also extended the 1mm radio light curve with the archival data from SMA available since 2002 (Gurwell et al. 2007) and the Polarimetric Monitoring of AGN at Millimeter Wavelengths (POLAMI, see Agudo et al. 2018b) program running at the 30m IRAM Millimeter Radio Telescope since 2010 (and at 3mm since 2006). The historical 1mm flux density and polarization degree light versus time are displayed in the bottom panels of Figure 2. From the 1mm flux density evolution, it is clear that this IXPE observing window coincides with the brightest total flux ever observed from BL Lac, with the two previous highest states, corresponding to two fast flares in 2012 and 2022, being a factor of 1.5 weaker than the late 2023 level. Comparison with the archival POLAMI observations reveals that the polarization degree in the 1mm band during this period was above the average value observed for this source.

We also analyzed a set of six ultra-high-angular resolution VLBA images from the 7mm BEAM-ME program[12] from 2023-10-13 to 2024-02-11; see Figure 9. The data were reduced, calibrated, imaged and model-fit as in Jorstad et al. (2017). The 7mm VLBA images show that there is a significant change of polarization angle in the VLBI core between November 6 and 25 from -24° to +53°. In agreement with the sharp total flux emission peak seen in the 1mm light curve (e.g., Fig. 2), these two VLBA observing epochs have the highest map peak of 15.14 and 16.24 Jy per beam, respectively, over all BEAM-ME observations started in June 2007. Nnote that the size of the beam is the same.) On 12 December, the polarization angle in the innermost jet region is $\sim 40°$, close to the optical median value. Also, the direction of this innermost jet region in Nov. 2023 is 42°, very close to the polarization angle in the optical and in the brightest VLBI core emission at 43 GHz on November 24. This behavior is consistent with that expected from a plane-perpendicular shock wave propagating from the innermost bent jet-regions in BL Lac just after the optical total flux and polarization flare reported in Figure 7. The close time coincidence of this millimeter-wave and optical

---

[12] See https://www.bu.edu/blazars/BEAM-ME.html/bllac.html

Table 4. Results of the spectral analysis performed over the different frequency bands, comparing the photon and spectral indices. The last column shows the number of energy bins N used for each fit.

Band	$\log \nu_{min}[Hz]$	$\log \nu_{max}[Hz]$	Photon index	Spectral index	N
Radio-mm	10	11	-0.55 ± 0.01	0.45 ± 0.01	13
mm-IR	11	13	-1.36 ± 0.08	-0.36 ± 0.08	7
IR-optical	12.2	14.8	-2.39 ± 0.01	-1.39 ± 0.01	4
Optical-UV	14	16	-2.82 ± 0.03	-1.82 ± 0.03	10
X-rays	16	19	-1.68 ± 0.01	-0.68 ± 0.01	23
γ rays	22.38	25.68	-2.31 ± 0.08	-1.31 ± 0.08	6

behavior strongly suggests that the site of the extreme optical behavior reported in this paper is in the VLBI core region in BL Lac.

E. BROAD-BAND SPECTRAL INDEX ANALYSIS

We have conducted an evaluation of the spectral indices of the different bands along the electromagnetic spectrum, finding further evidence for the leptonic SSC nature of the high-energy emission observed from BL Lac. For this, we have used the PYTHON package `JetSeT`[13] (Tramacere et al. 2009, 2011; Tramacere 2020), which contains an already implemented routine that allows calculation of the spectral (α) and photon indices (Γ, with $\Gamma = \alpha - 1$) in different frequency ranges of the electromagnetic spectrum through a power law fit. In particular, we have calculated the spectral indices in the radio to millimeter ($10^{10} - 10^{11}$ Hz), millimeter to IR ($10^{11} - 10^{13}$ Hz), IR to optical ($10^{12.2} - 10^{14.8}$ Hz), optical to UV ($10^{14} - 10^{16}$ Hz), X-rays ($10^{16} - 10^{19}$ Hz) and MeV to GeV ($10^{22.38} - 10^{25.38}$ Hz) bands. The derived spectral and photon index values are reported in Table 4. In Figure 3 we plot the flux density F_ν (in units of erg cm^{-2} s^{-1} Hz^{-1}) versus frequency, based on the spectral fits performed in each band.

Our broad-band spectral-index analysis clearly indicates that the optical and γ-ray spectrum have essentially the same slope, while the X-ray spectral index lies between the millimeter-to-IR and the IR-to-optical values. This is exactly the broad-band spectral behavior expected for an SSC scenario, where the γ rays are produced by Compton scattering of the optical synchrotron photons by the same electrons that emit the optical radiation, while the IR synchrotron photon field is the seed for the X-ray SSC emission, upscattered by the IR-emitting electrons.

REFERENCES

Abdo, A. A., Ackermann, M., Agudo, I., et al. 2010, ApJ, 716, 30, doi: 10.1088/0004-637X/716/1/30

Abdollahi, S., Acero, F., Ackermann, M., et al. 2020, ApJS, 247, 33, doi: 10.3847/1538-4365/ab6bcb

Abdollahi, S., Ajello, M., Baldini, L., et al. 2023, ApJS, 265, 31, doi: 10.3847/1538-4365/acbb6a

Agudo, I., Molina, S. N., Gómez, J. L., et al. 2012, in International Journal of Modern Physics Conference Series, Vol. 8, International Journal of Modern Physics Conference Series, 299–302, doi: 10.1142/S2010194512004746

Agudo, I., Thum, C., Ramakrishnan, V., et al. 2018a, MNRAS, 473, 1850, doi: 10.1093/mnras/stx2437

Agudo, I., Thum, C., Molina, S. N., et al. 2018b, MNRAS, 474, 1427, doi: 10.1093/mnras/stx2435

Aharonian, F. A. 2000, New Astronomy, 5, 377, doi: 10.1016/S1384-1076(00)00039-7

Ajello, M., Angioni, R., Axelsson, M., et al. 2020, ApJ, 892, 105, doi: 10.3847/1538-4357/ab791e

Atwood, W. B., Abdo, A. A., Ackermann, M., et al. 2009, ApJ, 697, 1071, doi: 10.1088/0004-637X/697/2/1071

Bachev, R., Tripathi, T., Gupta, A. C., et al. 2023, MNRAS, 522, 3018, doi: 10.1093/mnras/stad1063

Baldini, L., Bucciantini, N., Lalla, N. D., et al. 2022, SoftwareX, 19, 101194, doi: 10.1016/j.softx.2022.101194

Ballet, J., Burnett, T. H., Digel, S. W., & Lott, B. 2020, arXiv e-prints, arXiv:2005.11208, doi: 10.48550/arXiv.2005.11208

Bania, T. M., Marscher, A. P., & Barvainis, R. 1991, AJ, 101, 2147, doi: 10.1086/115836

Barniol Duran, R., Tchekhovskoy, A., & Giannios, D. 2017, MNRAS, 469, 4957, doi: 10.1093/mnras/stx1165

[13] https://jetset.readthedocs.io/en/latest/

Begelman, M. C., & Sikora, M. 1987, ApJ, 322, 650, doi: 10.1086/165760

Blackburn, J. K. 1995, in Astronomical Society of the Pacific Conference Series, Vol. 77, Astronomical Data Analysis Software and Systems IV, ed. R. A. Shaw, H. E. Payne, & J. J. E. Hayes, 367

Blandford, R., Meier, D., & Readhead, A. 2019, ARA&A, 57, 467, doi: 10.1146/annurev-astro-081817-051948

Blinov, D., Pavlidou, V., Papadakis, I., et al. 2018, MNRAS, 474, 1296, doi: 10.1093/mnras/stx2786

Blinov, D., Kiehlmann, S., Pavlidou, V., et al. 2021, MNRAS, 501, 3715, doi: 10.1093/mnras/staa3777

Bonometto, S., & Saggion, A. 1973, A&A, 23, 9

Burrows, D. N., Hill, J. E., Nousek, J. A., et al. 2005, SSRv, 120, 165, doi: 10.1007/s11214-005-5097-2

Dermer, C. D., & Schlickeiser, R. 1993, ApJ, 416, 458, doi: 10.1086/173251

Di Gesu, L., Tavecchio, F., Donnarumma, I., et al. 2022, AAS Meeting Abstracts, 662, A83, doi: 10.1051/0004-6361/202243168

Di Gesu, L., Marshall, H. L., Ehlert, S. R., et al. 2023, Nature Astronomy, 7, 1245, doi: 10.1038/s41550-023-02032-7

Di Marco, A., Costa, E., Muleri, F., et al. 2022, AJ, 163, 170, doi: 10.3847/1538-3881/ac51c9

Di Marco, A., Soffitta, P., Costa, E., et al. 2023, AJ, 165, 143, doi: 10.3847/1538-3881/acba0f

Escudero Pedrosa, J., Morcuende Parrilla, D., & Otero-Santos, J. 2024a, IOP4, v1.2.0, Zenodo, doi: 10.5281/zenodo.10222722

Escudero Pedrosa, J., Agudo, I., Morcuende, D., et al. 2024b, AJ, 168, 84, doi: 10.3847/1538-3881/ad5a80

Gabriel, C., Denby, M., Fyfe, D. J., et al. 2004, in Astronomical Society of the Pacific Conference Series, Vol. 314, Astronomical Data Analysis Software and Systems (ADASS) XIII, ed. F. Ochsenbein, M. G. Allen, & D. Egret, 759

Gehrels, N., Chincarini, G., Giommi, P., & et al. 2004, ApJ, 611, 38, doi: 10.1086/422091

Guan, X., Li, H., & Li, S. 2014, ApJ, 781, 48, doi: 10.1088/0004-637X/781/1/48

Gurwell, M. A., Peck, A. B., Hostler, S. R., Darrah, M. R., & Katz, C. A. 2007, in Astronomical Society of the Pacific Conference Series, Vol. 375, From Z-Machines to ALMA: (Sub)Millimeter Spectroscopy of Galaxies, ed. A. J. Baker, J. Glenn, A. I. Harris, J. G. Mangum, & M. S. Yun, 234

Harrison, F. A., Craig, W. W., Christensen, F. E., et al. 2013, ApJ, 770, 103, doi: 10.1088/0004-637X/770/2/103

Ho, P. T. P., Moran, J. M., & Lo, K. Y. 2004, ApJL, 616, L1, doi: 10.1086/423245

Hovatta, T., & Lindfors, E. 2019, NewAR, 87, 101541, doi: 10.1016/j.newar.2020.101541

Hovatta, T., Lindfors, E., Blinov, D., et al. 2016, A&A, 596, A78, doi: 10.1051/0004-6361/201628974

IceCube Collaboration, Aartsen, M. G., Ackermann, M., et al. 2018, Science, 361, 147, doi: 10.1126/science.aat2890

Jansen, F., Lumb, D., Altieri, B., et al. 2001, A&A, 365, L1, doi: 10.1051/0004-6361:20000036

Jethwa, P., Saxton, R., Guainazzi, M., Rodriguez-Pascual, P., & Stuhlinger, M. 2015, A&A, 581, A104, doi: 10.1051/0004-6361/201425579

Jorstad, S. G., Marscher, A. P., Larionov, V. M., et al. 2010, ApJ, 715, 362, doi: 10.1088/0004-637X/715/1/362

Jorstad, S. G., Marscher, A. P., Morozova, D. A., et al. 2017, ApJ, 846, 98, doi: 10.3847/1538-4357/aa8407

Kang, S., Lee, S.-S., & Byun, D.-Y. 2015, Journal of Korean Astronomical Society, 48, 257, doi: 10.5303/JKAS.2015.48.5.257

Kim, D. E., Di Gesu, L., Liodakis, I., et al. 2024, A&A, 681, A12, doi: 10.1051/0004-6361/202347408

Kislat, F., Clark, B., Beilicke, M., & Krawczynski, H. 2015, Astroparticle Physics, 68, 45, doi: 10.1016/j.astropartphys.2015.02.007

Kouch, P. M., Liodakis, I., Fenu, F., et al. 2024a, arXiv e-prints, arXiv:2411.16868. https://arxiv.org/abs/2411.16868

Kouch, P. M., Liodakis, I., Middei, R., et al. 2024b, arXiv e-prints, arXiv:2406.01693, doi: 10.48550/arXiv.2406.01693

Kraus, A., Krichbaum, T. P., Wegner, R., et al. 2003, A&A, 401, 161, doi: 10.1051/0004-6361:20030118

Krawczynski, H. 2012, ApJ, 744, 30, doi: 10.1088/0004-637X/744/1/30

Liodakis, I., Peirson, A. L., & Romani, R. W. 2019, ApJ, 880, 29, doi: 10.3847/1538-4357/ab2719

Liodakis, I., Marscher, A. P., Agudo, I., et al. 2022, Nature, 611, 677, doi: 10.1038/s41586-022-05338-0

Lott, B., Gasparrini, D., & Ciprini, S. 2020, arXiv e-prints, arXiv:2010.08406, doi: 10.48550/arXiv.2010.08406

Madejski, G. M., Sikora, M., Jaffe, T., et al. 1999, ApJ, 521, 145, doi: 10.1086/307524

Maraschi, L., Ghisellini, G., & Celotti, A. 1992, ApJL, 397, L5, doi: 10.1086/186531

Marrone, D. P., & Rao, R. 2008, in Proc. SPIE, Vol. 7020, Millimeter and Submillimeter Detectors and Instrumentation for Astronomy IV, ed. W. D. Duncan, W. S. Holland, S. Withington, & J. Zmuidzinas, 70202B, doi: 10.1117/12.788677

Marscher, A. P., & Gear, W. K. 1985, ApJ, 298, 114, doi: 10.1086/163592

Marscher, A. P., & Jorstad, S. G. 2022, Universe, 8, 644, doi: 10.3390/universe8120644

Marscher, A. P., Jorstad, S. G., D'Arcangelo, F. D., et al. 2008, Nature, 452, 966, doi: 10.1038/nature06895

Marshall, H. L. 2024, ApJ, 964, 88, doi: 10.3847/1538-4357/ad0897

Marshall, H. L., Liodakis, I., Marscher, A. P., et al. 2023, arXiv e-prints, arXiv:2310.11510, doi: 10.48550/arXiv.2310.11510

Middei, R., Liodakis, I., Perri, M., et al. 2023, ApJL, 942, L10, doi: 10.3847/2041-8213/aca281

Mondal, A., Sar, A., Kundu, M., Chatterjee, R., & Majumdar, P. 2025, ApJ, 978, 43, doi: 10.3847/1538-4357/ad9603

Myserlis, I., Angelakis, E., Kraus, A., et al. 2018, A&A, 609, A68, doi: 10.1051/0004-6361/201630301

Nagirner, D. I., & Poutanen, J. 1993, A&A, 275, 325

Nasa High Energy Astrophysics Science Archive Research Center (Heasarc). 2014, HEAsoft: Unified Release of FTOOLS and XANADU, Astrophysics Source Code Library, record ascl:1408.004

Nilsson, K., Pasanen, M., Takalo, L. O., et al. 2007, A&A, 475, 199, doi: 10.1051/0004-6361:20077624

Nilsson, K., Lindfors, E., Takalo, L. O., et al. 2018, A&A, 620, A185, doi: 10.1051/0004-6361/201833621

Otero-Santos, J., Piirola, V., Escudero Pedrosa, J., et al. 2024, AJ, 167, 137, doi: 10.3847/1538-3881/ad250d

Paliya, V. S., Zhang, H., Böttcher, M., et al. 2018, ApJ, 863, 98, doi: 10.3847/1538-4357/aad1f0

Panopoulou, G., Tassis, K., Blinov, D., et al. 2015, MNRAS, 452, 715, doi: 10.1093/mnras/stv1301

Peirson, A. L., Liodakis, I., & Romani, R. W. 2022, ApJ, 931, 59, doi: 10.3847/1538-4357/ac6a54

Peirson, A. L., & Romani, R. W. 2019, ApJ, 885, 76, doi: 10.3847/1538-4357/ab46b1

Peirson, A. L., Negro, M., Liodakis, I., et al. 2023, ApJL, 948, L25, doi: 10.3847/2041-8213/acd242

Pesce-Rollins, M., Lalla, N. D., Omodei, N., & Baldini, L. 2019, Nuclear Instruments and Methods in Physics Research A, 936, 224, doi: 10.1016/j.nima.2018.10.041

Piconcelli, E., Jimenez-Bailón, E., Guainazzi, M., et al. 2004, MNRAS, 351, 161, doi: 10.1111/j.1365-2966.2004.07764.x

Poutanen, J. 1994, ApJS, 92, 607, doi: 10.1086/192024

Primiani, R. A., Young, K. H., Young, A., et al. 2016, Journal of Astronomical Instrumentation, 5, 1641006, doi: 10.1142/S2251171716410063

Ramaprakash, A. N., Rajarshi, C. V., Das, H. K., et al. 2019, MNRAS, 485, 2355, doi: 10.1093/mnras/stz557

Ripperda, B., Liska, M., Chatterjee, K., et al. 2022, ApJL, 924, L32, doi: 10.3847/2041-8213/ac46a1

Roming, P. W. A., Kennedy, T. E., Mason, K. O., et al. 2005, SSRv, 120, 95, doi: 10.1007/s11214-005-5095-4

Shepherd, M. C. 1997, in Astronomical Society of the Pacific Conference Series, Vol. 125, Astronomical Data Analysis Software and Systems VI, ed. G. Hunt & H. Payne, 77

Shrestha, M., Steele, I. A., Piascik, A. S., et al. 2020, MNRAS, 494, 4676, doi: 10.1093/mnras/staa1049

Smith, P. S. 2017, The Astronomer's Telegram, 11047, 1

Smith, P. S., Montiel, E., Rightley, S., et al. 2009, 2009 Fermi Symposium, eConf Proceedings C091122, arXiv:0912.3621, doi: 10.48550/arXiv.0912.3621

Strüder, L., Briel, U., Dennerl, K., et al. 2001, A&A, 365, L18, doi: 10.1051/0004-6361:20000066

Telescope Array Collaboration, Abbasi, R. U., Allen, M. G., et al. 2023, Science, 382, 903, doi: 10.1126/science.abo5095

Tramacere, A. 2020, JetSeT: Numerical modeling and SED fitting tool for relativistic jets, Astrophysics Source Code Library, record ascl:2009.001

Tramacere, A., Giommi, P., Perri, M., Verrecchia, F., & Tosti, G. 2009, A&A, 501, 879, doi: 10.1051/0004-6361/200810865

Tramacere, A., Massaro, E., & Taylor, A. M. 2011, ApJ, 739, 66, doi: 10.1088/0004-637X/739/2/66

Weaver, Z. R., Williamson, K. E., Jorstad, S. G., et al. 2020, ApJ, 900, 137, doi: 10.3847/1538-4357/aba693

Weaver, Z. R., Jorstad, S. G., Marscher, A. P., et al. 2022, ApJS, 260, 12, doi: 10.3847/1538-4365/ac589c

Weisskopf, M. C., Soffitta, P., Baldini, L., et al. 2022, Journal of Astronomical Telescopes, Instruments, and Systems, 8, 026002, doi: 10.1117/1.JATIS.8.2.026002

Yang, H., Yuan, F., Li, H., et al. 2024, Science Advances, 10, eadn3544, doi: 10.1126/sciadv.adn3544

Zhang, H., & Böttcher, M. 2013, ApJ, 774, 18, doi: 10.1088/0004-637X/774/1/18

Zhang, H., Böttcher, M., & Liodakis, I. 2024, arXiv e-prints, arXiv:2404.12475, doi: 10.48550/arXiv.2404.12475

Zhang, H., Deng, W., Li, H., & Böttcher, M. 2016, ApJ, 817, 63, doi: 10.3847/0004-637X/817/1/63

Zhang, H., Fang, K., Li, H., et al. 2019, ApJ, 876, 109, doi: 10.3847/1538-4357/ab158d

Zhang, H., Li, H., Guo, F., & Taylor, G. 2017, ApJ, 835, 125, doi: 10.3847/1538-4357/835/2/125